

Modulation in the Air: Backscatter Communication over Ambient OFDM Carrier

Gang Yang, *Member, IEEE*, Ying-Chang Liang, *Fellow, IEEE*,
Rui Zhang, *Fellow, IEEE*, and Yiyang Pei, *Member, IEEE*

Abstract

Ambient backscatter communication (AmBC) enables radio-frequency (RF) powered backscatter devices (BDs) (e.g., sensors, tags) to modulate their information bits over ambient RF carriers in an over-the-air manner. This technology also called “modulation in the air”, thus has emerged as a promising solution to achieve green communications for future Internet-of-Things. This paper studies an AmBC system by leveraging the ambient orthogonal frequency division multiplexing (OFDM) modulated signals in the air. We first model such AmBC system from a spread-spectrum communication perspective, upon which a novel joint design for BD waveform and receiver detector is proposed. The BD symbol period is designed to be in general an integer multiplication of the OFDM symbol period, and the waveform for BD bit ‘0’ maintains the same state within a BD symbol period, while the waveform for BD bit ‘1’ has a state transition in the middle of each OFDM symbol period within a BD symbol period. In the receiver detector design, we construct the test statistic that cancels out the direct-link interference by exploiting the repeating structure of the ambient OFDM signals due to the use of cyclic prefix. For the system with a single-antenna receiver, the maximum-likelihood detector is proposed to recover the BD bits, for which the optimal threshold is obtained in closed-form expression. For the system with a multi-antenna receiver, we propose a new test statistic which is a linear combination of the per-antenna test statistics, and derive the corresponding optimal detector. The proposed optimal detectors require only knowing the strength of the backscatter channel, thus simplifying their implementation. Moreover, practical timing synchronization algorithms are proposed for the proposed AmBC system, and we also analyze the effect of various system parameters on the transmission rate and detection performance. Finally, extensive numerical results are provided to verify that the proposed transceiver design can improve the system bit-error-rate (BER) performance and the operating range significantly, and achieve much higher data rate, as compared to the conventional design.

Index Terms

Ambient backscatter communication (AmBC), orthogonal frequency division multiplexing (OFDM), spread spectrum, transceiver design, performance analysis, multi-antenna systems.

G. Yang is with the National Key Laboratory of Science and Technology on Communications, University of Electronic Science and Technology of China (UESTC), Chengdu, P. R. China (e-mail: yanggang@uestc.edu.cn).

Y.-C. Liang is with University of Electronic Science and Technology of China (UESTC), Chengdu, P. R. China (e-mail: liangyc@ieee.org). He is also with the Institute for Infocomm Research (I²R), A*STAR, Singapore.

R. Zhang is with the ECE Department, National University of Singapore (email: elezhang@nus.edu.sg).

Y. Pei is with Singapore Institute of Technology (email: yiyang.pei@singaporetech.edu.sg).

A preliminary version of this paper has been presented in [1].

I. INTRODUCTION

Wireless communication powered by ambient or dedicated radio-frequency (RF) source has drawn significant attention recently [2], [3]. In particular, ambient backscatter communication (AmBC) enables RF-powered backscatter devices (BDs) to harvest power from ambient RF signals (e.g., TV signal and WiFi signal), and to transmit information to nearby receivers (e.g., reader and smartphone) over the ambient RF carriers [4]. Thus, it has drawn significant attention from both academia and industry recently. Since AmBC is carried out at the same frequency band as the ambient wireless system, they can be viewed as a spectrum sharing system [5]. Different from traditional backscatter communication such as radio-frequency-identification (RFID) systems [6], AmBC can exempt the reader from generating RF sinusoidal carriers, thus enables low-cost and energy-efficient ubiquitous communications. It has also been verified that the harvested power from ambient RF signals could be sufficient to power a high-throughput battery-less sensor [7], [8]. Thus, AmBC is a promising technology for green communications with great potential for applications in next-generation Internet of Things (IoT) [9].

Due to the spectrum sharing nature, an inherent characteristic of the AmBC system is that the receiver suffers from strong direct-link interference out of the remote RF source. There are existing literature on receiver design for AmBC which treat the direct-link interference as part of the background noise [4], [10]–[12]. In [4], an averaging detector is proposed to decode the BD bits by treating the strong direct-link interference as noise, which results in very low decoding signal-to-noise-ratio (SNR) and thus low data rate. In [10] and [11], maximum-likelihood (ML) detection is studied for an AmBC system in which the BD adopts differential modulation. However, for the scenario where the backscatter channel is much weaker than the direct-link channel, which is typical in practice due to BD's small reflection coefficient and double-attenuation in the backscatter link, the proposed detection schemes suffer from severe performance degradation. An ambient WiFi backscatter system is proposed in [12], in which a WiFi helper (e.g., smartphone) decodes the BD bits by detecting the changes in received signal strength indication (RSSI). However, this system has very low data rate and very limited communication range (less than one meter), since the detection of the RSSI changes suffers from the strong direct-link interference from the WiFi access point (AP).

Moreover, there are other literature on receiver design for AmBC which cancel the direct-link interference by using signal processing methods [13]–[15]. In [13], the authors propose to use two receive antennas to cancel out the direct-link interference and thus increase the data rate. However, this interference cancellation scheme increases the complexity and cost of the receiver, and cannot be readily applied to a receiver with single or more than two antennas. A new WiFi backscatter system is proposed in [14], in which the WiFi AP decodes the received backscattered signal while

simultaneously transmitting WiFi packages to a standard WiFi client. This design relies on the self-interference-cancellation for full-duplex radios, resulting in high complexity and cost, thus cannot be applied to commercial WiFi APs with complexity and cost constraints. In [15], a backscatter device embeds its information on standard 802.11b packets by translating the originally transmitted 802.11b codeword to another valid 802.11b codeword. The detection WiFi AP first receives the original 802.11b packet decoded and sent by another WiFi AP, and then uses an XOR decoder to detect the information bit of the backscatter device. However, such detection relies on the collaboration of two WiFi APs, and this system is only applicable for the scenario of ambient 802.11b signal.

On the other hand, some recent work on AmBC address the problem of direct-link interference from the perspective of system design [16]–[18]. A passive WiFi system is proposed in [16], which requires a dedicated device to transmit RF sinusoidal carrier at a frequency that lies outside the desired WiFi channel, such that the WiFi receiver can suppress the resulting out-of-band (direct-link) carrier interference. However, the passive WiFi cannot be fully plugged-in and work with commodity devices, since it needs a dedicated device with specialized hardware to generate RF signal and perform carrier sensing. An inter-technology backscatter (interscatter) system is proposed in [17], which transforms wireless transmissions from one technology (e.g., Bluetooth) to another (e.g., WiFi) in the air. The BD creates frequency shifts on a single side of the carrier by using complex impedance of its backscatter circuit, so as to suppress the direct-link (carrier) interference and avoid a redundant copy on the opposite side of the carrier which exists in sideband modulation [16]. Similarly, a frequency-shifted backscatter (FS-Backscatter) system is proposed in [18] for on-body sensor applications, which reduces carrier interference by shifting the backscattered signal to a clean band that does not overlap with the carrier. However, the FS-Backscatter system cannot be applied to application scenarios where there is obvious temperature variability in the environment.

Also, there are some recent work on traditional backscatter communication systems [19]–[25], which use dedicated reader infrastructure to transmit RF sinusoidal carriers to power the passive tag and retrieve the tag information. The rate and reliability performance can be enhanced by using multi-antenna techniques. For instance, the bit-error-rate (BER) performance is analyzed for non-coherent frequency-shift-keying modulation in multi-input-single-output (MISO) fading channels [19], and the diversity-multiplexing trade-off is investigated in [20]. The reading range of RFID tags is improved by rectifier circuit design (see [21] and references therein), special waveform design [22] and energy beamforming [23]. In [25], the authors propose a network architecture that integrates wireless power transfer and backscatter communications, called wirelessly powered backscatter communication networks, and optimize the network coverage probability and transmission capacity by applying stochastic geometry. Recently, a bistatic architecture for backscatter communication is proposed in [24], i.e., the low-cost carrier emitter is detached from the reader, to increase the reading range.

While this bistatic backscatter communication system is similar to an AmBC system, this system requires to deploy and maintain a separate carrier emitter, which results in additional cost.

In this paper, we consider a new AmBC system over ambient orthogonal frequency division multiplexing (OFDM) modulated carriers in the air. OFDM is a widely used modulation scheme in current wireless systems such as WiFi and DVB [26], thus is a readily available ambient RF source. We aim to investigate system modelling, transceiver design and performance analysis for such AmBC system. The main contributions of this paper are summarized as follows:

- We first establish the system model for AmBC from a spread-spectrum (SS) communication perspective. We view the backscatter operation at the BD as an SS modulation technique, called “modulation in the air”, i.e., the backscattered signal is viewed as the multiplication of a low-rate BD data signal and a high-rate spreading signal (i.e., the received ambient signal at the BD from the RF source) in an over-the-air manner. However, the ambient backscatter system is different from traditional SS systems in the sense that the spreading codes are unknown and time varying, and the receiver suffers from strong direct-link interference from the RF source.
- Then, based on the established system model, we propose a novel joint design for BD waveform and receiver detector, which cancels out the direct-link interference. The BD symbol period is designed to be in general an integer multiplication of the OFDM symbol period, and the waveform for BD bit ‘0’ maintains the same state within a BD symbol period, while the waveform for BD bit ‘1’ has a state transition in the middle of each OFDM symbol period within a BD symbol period. With this new BD waveform design, we construct the test statistic for BD signal detection that cancels out the direct-link interference by exploiting the repeating structure of the ambient OFDM signals due to the use of cyclic prefix (CP). Our joint transceiver design cancels out direct-link interference without increasing the hardware complexity. To the best of our knowledge, this interference-cancellation scheme is proposed in this paper for the first time.
- Furthermore, we investigate the optimal detector design for the receiver in the considered AmBC system. For the case of single-antenna receiver, based on the constructed test statistic, the ML detector is derived, for which the optimal detection threshold is obtained in closed-form expression. For the case of multi-antenna receiver, we propose a new test statistic for BD signal detection, which is a linear combination of the per-antenna test statistics, each constructed from the received signal at one receive antenna. The corresponding optimal detector is then derived. To perform optimal detection, the receiver requires to estimate only the strength of the backscatter channel. This exempts the receiver from estimating the complete information of the direct-link and backscatter channels, which is challenging for the AmBC system, due to unknown ambient signal and strong direct-link interference.

- To implement the designed AmBC system, we propose efficient methods for estimating the essential parameters required. Specifically, the BD uses an autocorrelation-based method to estimate the propagation delay for the source-to-BD channel in a blind manner, and we propose a new algorithm to perform timing synchronization at the receiver. The proposed algorithm exempts the receiver from knowing the synchronization preambles in the ambient OFDM signals.
- Moreover, we analyze the effect of various system parameters including the CP length, number of subcarriers, detection SNR and maximum channel spread, on the transmission rate and detection performance of the AmBC system.
- Finally, extensive numerical results are provided to show that the proposed transceiver design can achieve much lower BER and higher data rate than the conventional design [4]. Also, numerical results show that the proposed timing synchronization methods are practically valid and efficient, and the deployment of multiple antennas at the receiver can improve the BER performance as well as the operating range significantly.

Organizations: The rest of this paper is organized as follows. Section II presents the system model for AmBC over ambient OFDM carriers in the air. Section III first presents the spread-spectrum based signal model, and then proposes the optimal joint transceiver design for the BD waveform and the receiver detector in a single-antenna system. Section IV presents practical methods for estimating essential parameters for implementing AmBC systems. Section V further investigates the optimal receiver design for the case of multi-antenna receiver. Section VI analyzes the effect of various system parameters on the transmission rate and detection performance. Section VII presents the numerical results. Finally, Section VIII concludes the paper.

Notations: The main notations in this paper are listed as follows. $|\cdot|$ means the operation of taking the absolute value. \otimes stands for the convolution operation of two signals. $\mathcal{N}(\mu, \sigma^2)$ denotes the real Gaussian distribution with mean μ and variance σ^2 . $\mathcal{CN}(\mu, \sigma^2)$ denotes the circularly symmetric complex Gaussian (CSCG) distribution with mean μ and variance σ^2 . $\mathcal{Q}(x)$ denotes the \mathcal{Q} -function, i.e., $\mathcal{Q}(x) = \frac{1}{\sqrt{2\pi}} \int_x^\infty e^{-r^2/2} dr$. $\mathbb{E}[\cdot]$ denotes the statistical expectation. $\lfloor \cdot \rfloor$ denotes the floor operation.

II. SYSTEM MODEL AND PROTOCOL DESCRIPTION

In this section, we present the system model and describe the link-layer protocol for the AmBC system over ambient OFDM carriers in the air.

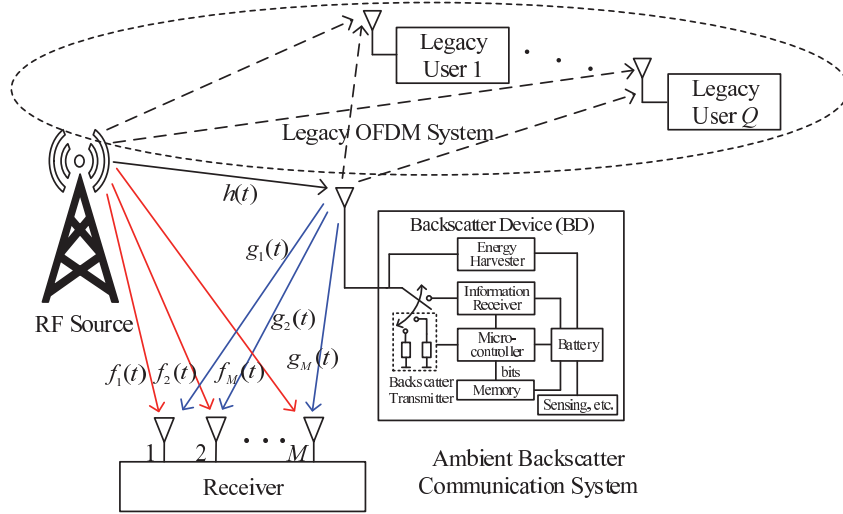


Fig. 1: System model for ambient backscatter communications over OFDM carriers in the air.

A. System Model

As illustrated in Fig. 1, we consider two co-existing communication systems: the legacy¹ OFDM system which consists of an RF source (e.g., TV tower, WiFi AP) and its dedicated (legacy) users (e.g., TV receiver, WiFi client), and the AmBC system which consists of a BD with RF-power harvesting module and a receiver (e.g., reader in RFID systems) equipped with in general M ($M \geq 1$) antennas. The RF source transmits OFDM signals to the legacy users. We are interested in the AmBC system in which the BD transmits its modulated signals to the receiver over the ambient OFDM carrier from the RF source. The BD contains a single backscatter antenna, a backscatter transmitter (i.e., a switched load impedance), an energy harvester, an information receiver², a micro-controller, a memory, a rechargeable battery replenished by the energy harvester, and other modules (e.g., sensing). The energy harvester collects energy from ambient OFDM signals and uses it to replenish the battery which provides power for all modules of the BD. To transmit information bits stored in the memory to the receiver, the BD modulates its received ambient OFDM carrier by intentionally switching the load impedance to change the amplitude and/or phase of its backscattered signal, and the backscattered signal is received and finally decoded by the receiver. Also, the BD antenna can be switched to the information receiver which is able to perform information decoding and other simple signal processing operations.

As shown in Fig. 1, for the channel between the RF source and the BD, we denote $h(t)$ as the (baseband) channel impulse response (CIR) with multi-path spread τ_h , and d_h as the channel

¹Hereinafter, the term “legacy” refers to existing wireless communication systems, such as DVB, cellular and WiFi systems.

²In practice, the simple BD can adopt the direct-conversion structure for information receiver, which is of low hardware-complexity, small size and low power [27]. It can further use ultra low-power analog-to-digital converter to reduce power consumption.

propagation delay which is the arrival time of the first path of $h(t)$, respectively. Similarly, we denote $g_m(t)$ as the CIR with multi-path spread τ_g and propagation delay d_g between the BD and the m -th receive antenna at the receiver, and $f_m(t)$ as the CIR with multi-path spread τ_f and propagation delay d_f between the RF source and the m -th receive antenna at the receiver, respectively. The corresponding passband channels are denoted as $\tilde{f}_m(t)$'s, $\tilde{h}(t)$, and $\tilde{g}_m(t)$'s, respectively. The backscatter channel is a concatenation of the source-to-BD channel and the BD-to-receiver channel. For convenience, we define the total channel spread for each channel as the sum of its multi-path spread and its channel propagation delay. We assume that the relevant channels are independent from each other, which is a typical assumption in the literature such as [19], [23], and [28].

1) *Continuous-time Signal Model:* For the AmBC system, we first establish the model for continuous-time signals. Denote the passband signal transmitted from the RF source by

$$\tilde{s}(t) \triangleq \text{Re} \{ \sqrt{p}s(t)e^{j2\pi f_c t} \}, \quad (1)$$

where $s(t)$ is the baseband OFDM signal with unit power, p is the average transmit power, and f_c represents the carrier frequency of the RF source.

Let N be the number of subcarriers of the OFDM signal $s(t)$. In order to combat the inter-symbol-interference (ISI), a CP is added at the beginning of each OFDM symbol, and the CP length t_c is set to be longer than the maximum channel spread of all legacy OFDM receivers [26]. Typically, compared to the legacy OFDM receivers, the AmBC system is deployed in a place relatively close to the RF source, such that the BD can harvest more energy from the RF source. Based on this deployment criterion, we have two practical assumptions. First, we assume that the CP length t_c is much longer than the maximum channel spread of AmBC system. Second, we assume that the energy from the rechargeable battery at the BD is sufficient for its operation, and focus on the transceiver design for AmBC, for the purpose of exposition.

From Fig. 1 and (1), the ambient OFDM signal received at the BD can be represented by using the baseband signal $s(t)$ and the baseband channel $h(t)$ [26], i.e.,

$$\tilde{c}(t) = \text{Re} \{ [\sqrt{p}s(t - d_h) \otimes h(t)] e^{j2\pi f_c(t - d_h)} \}. \quad (2)$$

Thus the corresponding baseband signal received at the BD is

$$c(t) = \sqrt{p}s(t - d_h) \otimes h(t). \quad (3)$$

Let $x(t)$ be the BD's baseband signal to be transmitted. Denote α as the complex attenuation (i.e., reflection coefficient) of the signal $\tilde{c}(t)$ inside the BD, which depends on the antenna impedance and the load impedance of the BD. Then the backscattered signal out of the BD is $\alpha\tilde{c}(t)x(t)$, where α controls the power of the backscattered signal by the BD.

Remark 1. The above operation of backscattering can be viewed as a new modulation technique for wireless communication systems. The incident passband signal $\tilde{c}(t)$, which is from the air, plays the role of carrier signal, and the BD signal $x(t)$ is the baseband modulation signal. We call the technique of modulating the BD signal $x(t)$ to the carrier $\tilde{c}(t)$ as “modulation in the air”, which exempts the BD from generating RF sinusoidal carriers locally and thus significantly reduces its hardware complexity and power consumption.

The received passband signal at the m -th antenna, $m = 1, 2, \dots, M$, of the receiver is thus

$$\tilde{y}_m(t) = [\alpha\tilde{c}(t - d_g)x(t - d_g)] \otimes \tilde{g}_m(t) + \tilde{s}(t - d_f) \otimes \tilde{f}_m(t) + \tilde{w}_m(t), \quad (4)$$

where $\tilde{w}_m(t)$ is the passband noise at the receiver. After down-conversion to baseband, the received baseband signal at the receiver is written as

$$y_m(t) = y_{b,m}(t) + y_{d,m}(t) + w_m(t), \quad (5)$$

where $y_{b,m}(t) = [\alpha c(t - d_g)x(t - d_g)] \otimes g_m(t)$ is the received backscattered signal from the BD, $y_{d,m}(t) = \sqrt{p}s(t - d_f) \otimes f_m(t)$ is the direct-link interference from the RF source, and $w_m(t)$ is the equivalent baseband additive white Gaussian noise (AWGN) with power σ^2 , i.e., $w_m(t) \sim \mathcal{CN}(0, \sigma^2)$. We assume that the noise term $w_m(t)$ is independent of the signals $y_{d,m}(t)$ and $y_{b,m}(t)$.

Due to short BD-to-receiver distance in practice, we assume that each channel $g_m(t)$ has a single path, denoted by g_m . The received backscattered signal at the m -th antenna of the receiver is thus simplified as

$$y_{b,m}(t) = \alpha g_m c(t - d_g)x(t - d_g) = \alpha g_m \sqrt{p}s(t - d_h - d_g) \otimes h(t - d_g)x(t - d_g). \quad (6)$$

Remark 2. Since the AmBC is carried out at the same frequency band as the legacy OFDM system, the whole system in Fig. 1 can be considered as a spectrum sharing system [5], [29]. The backscattered signal $\alpha\tilde{c}(t)x(t)$ is also received by each nearby legacy OFDM user through the channel from the BD to the legacy user, resulting in interference to the legacy OFDM system. However, the power of this resulting interference is typically much lower than that of the received signal from the RF source, even if the legacy users and the BD are close to each other. The reason is two-fold. First, the absolute value of reflection coefficient α is typically very small [6]. Second, the received signal from the RF source suffers from one-round channel attenuation, while the interference signal (i.e., backscattered signal) suffers from two-round channel attenuation, i.e., the source-to-BD channel and the BD-to-legacy-user channel. In a similar argument, at the side of the receiver in the AmBC system, the direct-link interference from the RF source is also typically much stronger than the backscattered signal from the BD, which makes the BD signal detection a challenging task.

2) *Discrete-time Signal Model*: Let f_s be the sampling rate (or equivalently, the one-sided bandwidth) of the ambient OFDM signal. The discrete-time propagation delays for all channels are thus denoted as $D_h = \lfloor d_h f_s \rfloor$, $D_g = \lfloor d_g f_s \rfloor$ and $D_f = \lfloor d_f f_s \rfloor$, respectively. Denote the propagation delay of the backscatter channel by $D_b = \lfloor (d_h + d_g) f_s \rfloor$. Define the minimum channel propagation delay as $D = \min\{D_f, D_b\}$. Since $d_h \gg d_g$ in practice, we assume that $D_b \approx D_h$. Similarly, the discrete-time total channel spreads are denoted as $L_h = \lfloor (d_h + \tau_h) f_s \rfloor$, $L_g = \lfloor (d_g + \tau_g) f_s \rfloor$ and $L_f = \lfloor (d_f + \tau_f) f_s \rfloor$, respectively. Denote the total channel spread of the backscatter channel by $L_b = \lfloor (d_h + \tau_h + d_g + \tau_g) f_s \rfloor$. Define the maximum channel spread as $L = \max\{L_f, L_b\}$.

For convenience, we rewrite the discrete-time source signal, received signal at the BD, and the BD signal as $s[n] = s(n/f_s)$, $c[n] = c(n/f_s)$, and $x[n] = x(n/f_s)$, respectively. After analog-to-digital conversion, the discrete-time representation of the received signal at the receiver is

$$y_m[n] = y_{b,m}[n] + y_{d,m}[n] + w_m[n], \quad (7)$$

where $y_{b,m}[n] = \alpha c[n - D_g]x[n - D_g] \otimes g_m[n]$, $y_{d,m}[n] = \sqrt{p}s[n - D_f] \otimes f_m[n]$, and $w_m[n] \sim \mathcal{CN}(0, \sigma^2)$. The relevant discrete-time signals are illustrated in Fig. 4 in Section III.

For the studied AmBC system, our objective is to design the BD waveform and receiver detector to recover the BD signal $x[n]$ from the received signals $y_m[n]$'s at the receiver, without knowing the ambient signal $\sqrt{p}s[n]$ transmitted from the RF source. In the rest of this paper, we use the baseband signals and the baseband CIRs, for clarity of description. Before designing the transceiver, we propose a protocol for the AmBC system to operate in practice.

B. Link-layer Protocol Design

As illustrated in Fig. 2, the proposed protocol adopts frame-based transmission, where each BD frame with (discrete) time duration T_f consists of four phases, the wake-up-preamble transmission (WUPT) phase with time duration T_w , the blind timing synchronization (BTS) phase with time duration T_b , the training-preamble transmission (TPT) phase with time duration T_t , and the device data transmission (DDT) phase with time duration T_d . The BD by default is in a sleep mode to save energy if it has no data to transmit. Once it has enough data to transmit, the BD is activated. In the following, we specify the operations in each phase.

- In the first WUPT phase, the BD is switched into the backscatter transmitter, and the BD sends a specialized preamble to activate the receiver's hardware. As in the literature [4], [12], [17], a short sequence of alternating '1' and '0' can be used as the wake-up preamble. The power consumption of the receiver can be saved via this event-driven wake-up scheme.
- In the second BTS phase, the BD switches its antenna into the information receiver and estimates the channel propagation delay D_h from the RF source. The BD performs blind timing estimation

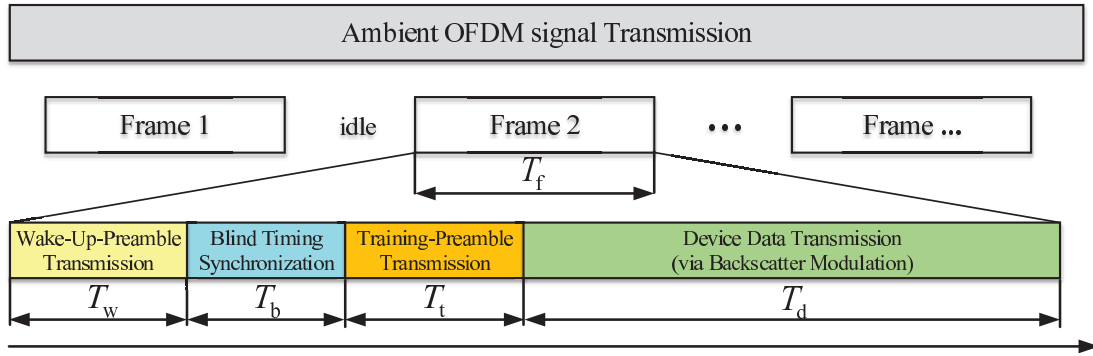


Fig. 2: Protocol design for AmBC system.

by exploiting the CP structure of $s[n]$, since it does not know the ambient OFDM signal $s[n]$. The blind estimation algorithm will be presented in Section IV-A.

- In the third TPT phase, the BD switches its antenna into the backscatter transmitter, and chooses the estimate of D_h as the starting time to send a training preamble known by the receiver. The receiver receives both the direct-link signal $y_d[n]$ and the preamble signal backscattered from the BD. Then the receiver estimates essential parameters including the minimum propagation delay D and the maximum channel spread L , as well as the average signal power σ_u^2 when the BD is backscattering. Such estimation algorithms will be presented in Section IV-B.
- In the fourth DDT phase, the BD switches its antenna into the backscatter transmitter, and transmits data bits to the receiver. Both the BD waveform and the receiver detector will be studied in Section III in detail.

The time allocations for BTS and TPT phases affect both the parameter estimation accuracy and the communication throughput in the DDT phase. The effect on parameter estimation will be numerically investigated in Section VII. However, this paper focuses on the transceiver design, and will not derive the optimal timing allocation for all phases, due to the space limitation.

III. TRANSCEIVER DESIGN FOR SINGLE-ANTENNA SYSTEM

In this section, we establish a spread-spectrum (SS) model for the general signal model in (7), based on which we study the transceiver design, including the BD waveform design and the optimal receiver detector, for an AmBC system with a single-antenna receiver, i.e. $M = 1$.

A. A Spread-Spectrum Perspective for Signal Model

Since the switching frequency of backscatter state at the BD is typically much smaller than the OFDM sampling rate f_s [6], the signal backscattered by the BD can be viewed as the multiplication of a low-rate BD data signal $x[n]$ scaled by the reflection coefficient α , and the high-rate spreading-code signal $c[n]$ in an over-the-air manner. The chip duration of this spreading code is equal to the

sampling period of the received OFDM signal $c[n]$, which is much shorter than the duration of each BD symbol. Suppose that the BD symbol duration is designed to be equal to N_0 OFDM sampling periods (i.e., N_0/f_s), the processing gain (or spreading factor), denoted by G , is then $G = N_0$, and the data rate of BD transmission is $\frac{f_s}{N_0}$. Hence, the BD symbol period needs to be designed carefully to achieve the optimal trade-off between the processing gain and the data rate.

Different from traditional SS communication systems, there are three main challenges for the receiver to detect the BD signal $x[n]$ from its received signals $y_m[n]$'s, which are listed as follows:

- First, the spreading code $c[n]$ depends on the unknown ambient signal $\sqrt{p}s[n]$ and the fading channel $h[n]$, thus is time-varying, and unknown to the receiver. Therefore, the traditional correlation detection cannot be applied to the considered system.
- Second, the received direct-link interference signals $y_{d,m}[n]$'s are typically unknown by the receiver and much stronger than the received backscattered signals $y_{b,m}[n]$'s, resulting in very low signal-to-interference-noise ratio (SINR) for the receiver if they are treated as part of the background noise.
- Third, due to unknown ambient signal $\sqrt{p}s[n]$ and strong direct-link interferences $y_{d,m}[n]$'s, it is challenging for the receiver to estimate all the fading channels $h[n]$, g_m 's and $f_m[n]$'s. Hence, coherent detection cannot be applied to the considered system.

To solve the above challenging problems, in the rest of this section, we focus on the joint transceiver design for the AmBC system with a single-antenna receiver. For notational simplicity, the subscript $m = 1$ is omitted in the rest of this section.

B. BD Waveform Design

Specifically, we can design the time duration of each BD symbol to be equal to K ($K \geq 1$) OFDM symbol periods each of which consists of $(N + N_c)$ sampling periods, i.e., the spreading gain is $G = K(N + N_c)$. As shown in Fig. 3, the BD uses the following waveform $x[n]$ to convey information bit $B = 1$ in each BD symbol,

$$x[n] = \begin{cases} 1, & \text{for } n = (k-1)(N + N_c), \dots, (k-1)(N + N_c) + \frac{N+N_c}{2} - 1, \\ -1, & \text{for } n = (k-1)(N + N_c) + \frac{N+N_c}{2}, \dots, k(N + N_c) - 1, \end{cases} \quad (8)$$

for $k = 1, \dots, K$, where for convenience we assume that $(N + N_c)$ is an even integer. The following waveform $x[n]$ is then used to convey information bit $B = 0$ in each BD symbol,

$$x[n] = 1, \text{ for } n = 0, \dots, K(N + N_c) - 1. \quad (9)$$

That is, for bit '1', there is a state transition in the middle of each OFDM symbol period within one BD symbol period, while for bit '0', there is no such transition.

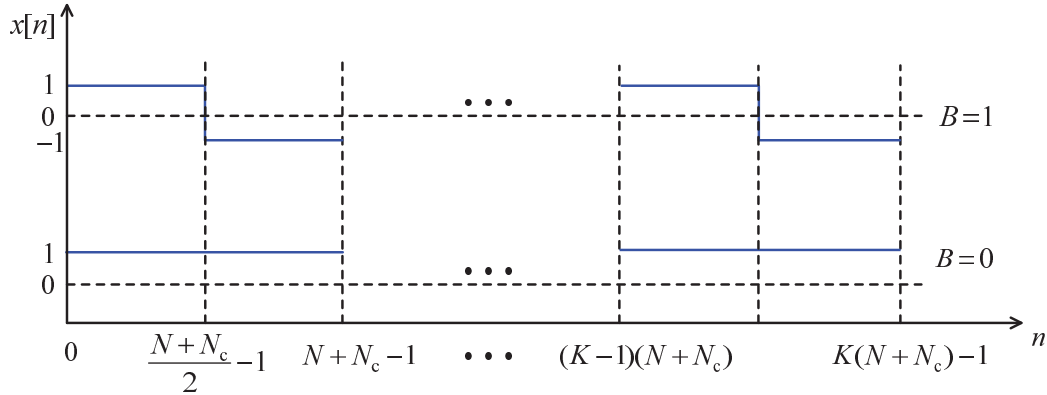


Fig. 3: BD waveform design.

Remark 3. The waveform design in (8) and (9) aims to enable the receiver to cancel out the strong direct-link interference, as will be shown in the next subsection. Also the designed waveform can be easily implemented in simple and low-cost BDs, since it is similar to FM0 waveform widely used in commercial RFID tags [6].

C. Receiver Detection Design

In this subsection, we study the detector design at the receiver. For convenience, we choose $K = 1$, without loss of generality.

1) *Construction of Test Statistic:* As characterized in (7) for $m = 1$, the direct-link signal $y_d[n]$ and the backscatter-link signal $y_b[n]$ experience different multi-paths $f_m[n]$ and $h[n]g_m$, respectively. However, both $y_d[n]$ and $y_b[n]$ have its repeating structure, which are illustrated in Fig. 4, since the CP is inserted at the beginning of each OFDM symbol of the RF source signal $s[n]$.

To be specific, as illustrated in Fig. 4, due to the use of CP and the multi-path effect, two portions of the received signal from the RF source, $y_d[n]$, in each OFDM symbol period at the receiver are identical, i.e.,

$$y_d[n] = y_d[n + N], \quad n = L_f - 1, \dots, N_c + D_f - 1. \quad (10)$$

Similarly, the repeating structure holds for the received signal at the BD, $c[n]$, i.e.,

$$c[n] = c[n + N], \quad n = L_h - 1, \dots, N_c + D_h - 1. \quad (11)$$

From (8), (9), and (11), the received backscatter-link signal $y_b[n]$ at the receiver has the following repeating structure,

$$y_b[n] = \begin{cases} y_b[n + N], & \text{if } B = 0, \\ -y_b[n + N], & \text{if } B = 1. \end{cases} \quad (12)$$

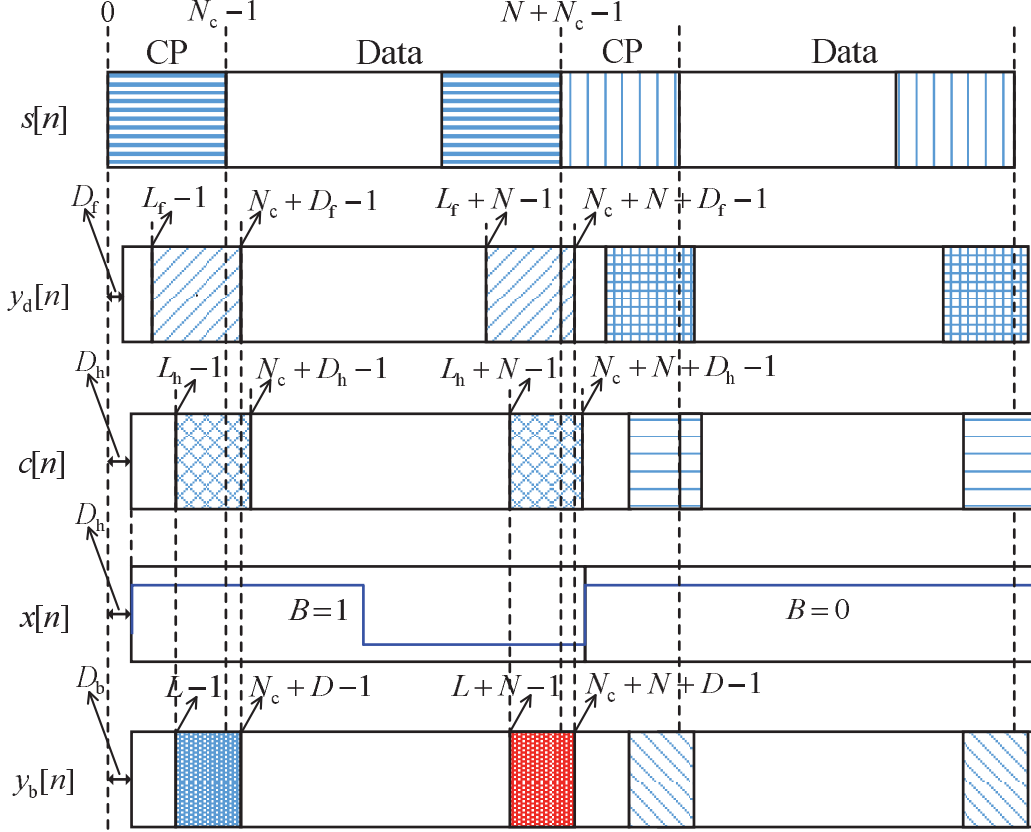


Fig. 4: Signal structure for the case of $D_f < D_h$ and $L_f < L_h$.

for $n = L_b - 1, \dots, N_c + D_b - 1$.

By utilizing the repeating structure of $y_d[n]$ in (10) and $y_b[n]$ in (12), we further have

$$z[n] \triangleq y[n] - y[n+N] = \begin{cases} v[n], & \text{if } B = 0, \\ u[n] + v[n], & \text{if } B = 1, \end{cases} \quad (13)$$

for $n = L - 1, \dots, N_c + D - 1$, where the signal $u[n]$ and the noise $v[n]$ are given as follows, respectively,

$$u[n] = 2\alpha g \sqrt{p} \sum_{l=0}^{L_h-1} s[n-l] h[l], \quad (14)$$

$$v[n] = w[n] - w[n+N]. \quad (15)$$

Clearly, the noise $v[n] \sim \mathcal{CN}(0, \sigma_v^2)$ with power³ $\sigma_v^2 = 2\sigma^2$.

For large N , the received OFDM signal $c[n]$ at the BD is a sequence of independent and identically distributed (i.i.d.) random variables each of which follows the CSCG distribution with zero mean and

³The receiver can estimate σ_v^2 offline, since σ_v^2 depends on only the noise variance.

variance $p \sum_{l=0}^{L_h-1} |h[l]|^2$ [26], [30]. Hence, the signal $u[n] = 2\alpha g c[n]$ is a sequence of independent random variables each of which is identically distributed as $u[n] \sim \mathcal{CN}(0, \sigma_u^2)$, where the variance σ_u^2 is given by

$$\sigma_u^2 = 4p|\alpha|^2|g|^2 \sum_{l=0}^{L_h-1} |h[l]|^2. \quad (16)$$

For notational simplicity, we define the detection SNR as

$$\gamma \triangleq \frac{\sigma_u^2}{\sigma_v^2} = \frac{2p|\alpha|^2|g|^2 \sum_{l=0}^{L_h-1} |h[l]|^2}{\sigma^2}. \quad (17)$$

Notice that there is a trade-off between the detection SNR γ in (17) and the power available for harvesting at the BD. When the reflection coefficient α increases, the detection SNR γ increases, but the available power for harvesting decreases [20], due to energy conservation law, and vice versa.

Remark 4. We have two observations for the constructed intermediate signal $z[n]$ in (13). First, in $z[n]$, the direct-link interference $y_d[n]$ is completely cancelled out, and only the received backscattered signal $y_b[n]$ remains if $B = 1$. This leads to higher detection SNR γ , thus tackles the challenge of strong direct-link interference at the receiver. Second, the statistic of the signal $u[n]$ (i.e., the signal power σ_u^2) hinges on only the strength of the overall backscatter channel $\alpha g h[n]$'s, independent of the phase information of g and $h[n]$'s. This exempts the receiver from estimating the individual channels g and $h[n]$'s, thus tackles the challenge of channel estimation at the receiver.

For convenience of analysis, we define the repeating length of the constructed signal $z[n]$ in (13) as $J \triangleq N_c + D - L + 1$. Since both the signal $u[n]$ and the noise $v[n]$ are CSCG, the optimal detector is the energy detector [31]. Therefore, we construct the following test statistic,

$$R = \frac{1}{J\sigma_v^2} \sum_{n=L-1}^{N_c+D-1} |z[n]|^2. \quad (18)$$

Clearly, for general case of arbitrary $J \geq 1$, the exact distribution of R is Chi-square distribution with degrees of freedom $2J$. When the number of summation terms in (18) (i.e., J) is large⁴, the central limit theorem (CLT) [32] implies that the distribution of R can be approximated by the Gaussian distribution, which is given by the following lemma.

Lemma 1. When the repeating length J is large, the conditional distribution of the test statistic R

⁴Note that in practice J can be effectively made arbitrarily large by increasing the spreading gain parameter, K , even with finite N_c , L and D values.

is given by

$$R = \begin{cases} R|_{B=0} \sim \mathcal{N}(\mu_0, \sigma_0^2), & \text{if } B = 0, \\ R|_{B=1} \sim \mathcal{N}(\mu_1, \sigma_1^2), & \text{if } B = 1, \end{cases} \quad (19)$$

where the mean values are

$$\mu_0 = 1, \quad \mu_1 = \gamma + 1, \quad (20)$$

and the variance values are

$$\sigma_0^2 = \frac{1}{J}, \quad \sigma_1^2 = \frac{(\gamma + 1)^2}{J}. \quad (21)$$

Proof: The proof is based on the CLT, and follows similar steps as in [30]. Please refer to Appendix A. ■

2) *Optimal Detector Design:* Let $p(R|_{B=0})$ and $p(R|_{B=1})$ be the probability density function (PDF) of the conditional random variable $R|_{B=0}$ and $R|_{B=1}$, respectively. Since $B = 0$ and $B = 1$ are equally probable, the optimal detector follows the ML rule [31], i.e.,

$$\hat{B} = \begin{cases} 0, & \text{if } p(R|_{B=0}) > p(R|_{B=1}), \\ 1, & \text{if } p(R|_{B=1}) > p(R|_{B=0}). \end{cases} \quad (22)$$

In other words, the decision rule is $\hat{B} = 0$ if $R < \epsilon$, and $\hat{B} = 1$ otherwise, where ϵ is the detection threshold. From (19), the BER is

$$P_e(\epsilon) = \frac{1}{2}P(\hat{B} = 1|B = 0) + \frac{1}{2}P(\hat{B} = 0|B = 1) = \frac{1}{2}P_{\text{fa}}(\epsilon) + \frac{1}{2}P_{\text{md}}(\epsilon), \quad (23)$$

where the probability of false alarm $P_{\text{fa}}(\epsilon)$ and the probability of missing detection $P_{\text{md}}(\epsilon)$ are given as follows, respectively,

$$\begin{aligned} P_{\text{fa}}(\epsilon) &= \mathcal{Q}\left(\frac{\epsilon - \mu_0}{\sqrt{\sigma_0^2}}\right) = \mathcal{Q}\left(\sqrt{J}(\epsilon - 1)\right), \\ P_{\text{md}}(\epsilon) &= \mathcal{Q}\left(\frac{\mu_1 - \epsilon}{\sqrt{\sigma_1^2}}\right) = \mathcal{Q}\left(\sqrt{J}\left(1 - \frac{\epsilon}{\gamma + 1}\right)\right). \end{aligned} \quad (24)$$

The BER is illustrated as the shadow area in Fig. 5.

Hence, the optimal threshold ϵ^* is the solution to the following problem

$$(P1) \quad \min_{\epsilon} P_e(\epsilon) = \frac{1}{2}\mathcal{Q}\left(\sqrt{J}(\epsilon - 1)\right) + \frac{1}{2}\mathcal{Q}\left(\sqrt{J}\left(1 - \frac{\epsilon}{\gamma + 1}\right)\right) \quad (25a)$$

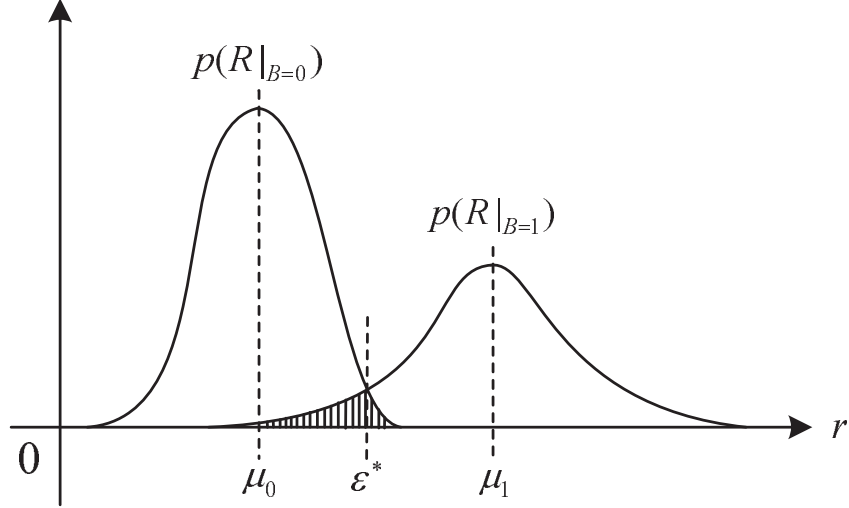


Fig. 5: Two conditional PDFs and the corresponding BER region (shadow area).

$$\text{s. t. } \epsilon > 0. \quad (25\text{b})$$

The optimal threshold ϵ^* and the corresponding minimum BER $P_{e,\min}$ are given in the following theorem.

Theorem 1. *The optimal detection threshold for the ML detector in (22) is given by*

$$\epsilon^* = \frac{\gamma + 1}{\gamma(\gamma + 2)} \left(\gamma + \sqrt{\gamma^2 + \frac{2\gamma(\gamma + 2) \ln(\gamma + 1)}{J}} \right). \quad (26)$$

And the corresponding minimum BER is given by

$$P_{e,\min} = \frac{1}{2} \mathcal{Q} \left(\sqrt{J}(\epsilon^* - 1) \right) + \frac{1}{2} \mathcal{Q} \left(\sqrt{J} \left(1 - \frac{\epsilon^*}{\gamma + 1} \right) \right). \quad (27)$$

Proof: Please refer to Appendix B. ■

Remark 5. From Theorem 1, we have two observations. First, the optimal detection threshold ϵ^* decreases as the repeating length J increases. Also, $\epsilon^* \rightarrow \frac{2(\gamma+1)}{\gamma+2}$, as $J \rightarrow \infty$. It can be easily checked that the limiting threshold ϵ^* is located in the closed interval between the two conditional mean values μ_0 and μ_1 , due to $\gamma \geq 0$. Second, from Theorem 1, we observe that given J , the optimal detection threshold and the corresponding minimum BER depend on only the detection SNR γ , being irrelevant to the number of subcarriers N . This is because only the CP-induced repeating parts of the received signal is utilized to detect the BD information bits, without using other parts in each OFDM symbol period.

Remark 6. Although the derivation of BER and the detection threshold follows similar steps as standard binary detection [33], our system model, BD signal design and test statistics construction

are fundamentally different from existing literature on BER analysis for AmBC [10], [11].

IV. PARAMETER ESTIMATION FOR AMBC SYSTEMS

In this section, we present practical methods for estimating essential parameters for implementing AmBC systems. In practice, the BD and the receiver can estimate basic parameters from the received OFDM signals. For instance, they can estimate N as the distance of two adjacent peaks of the autocorrelation of the received signal.

A. Timing Estimation for BD

In the BTS phase, the BD is switched into information receiver mode and estimates the channel propagation delay D_h , which is required for the proposed modulation at the BD as in (8) and (9). For the case in which the BD knows the synchronization preamble in the ambient OFDM signals⁵, it can estimate D_h accurately by using traditional estimation methods such as cross-correlation based method or other algorithms reviewed in [35].

For the case in which the BD does not know the synchronization preamble, it can still use its received incident signal $c[n]$ to estimate D_h by utilizing the repeating CP structure. Specifically, the BD performs autocorrelation for the received signals within the time window of K_1 ($K_1 \geq 1$) OFDM symbol periods, i.e., $T_b = K_1(N + N_c)$, and estimates D_h as

$$\widehat{D}_h = \frac{1}{K_1} \arg \max_{d=0, \dots, N_c-1} \sum_{k=0}^{K_1-1} \sum_{n=0}^{N_c-1} \frac{\left| c[n+d+k(N+N_c)] c^*[n+d+N+k(N+N_c)] \right|}{\left| c[n+d+N+k(N+N_c)] \right|^2}. \quad (28)$$

B. Parameter Estimation for Receiver

We first consider timing synchronization for the case in which the receiver knows the synchronization preamble in the ambient OFDM signals. The receiver can use cross-correlation based method to estimate the direct-link propagation delay D_f and the backscatter-link propagation delay D_b accurately, in the BTS phase and the TPT phase, respectively. Then it can obtain an estimate of $D = \min\{D_f, D_b\}$. While in the TPT phase, it also obtains the estimated maximum channel spread L by estimating the maximum multi-path delay in the frequency domain [35], in which the backscatter link is treated as additional multi-path.

Second, we consider timing synchronization for the case in which the receiver does not know the synchronization preamble. In the TPT phase, the BD is switched into backscattering mode and

⁵This is practical in some scenarios. For instance, for WLAN systems with 802.11a standard [34], fixed frequency-domain OFDM symbols generate a synchronization preamble which consists of several identical training symbols.

the receiver estimates the minimum channel propagation delay D and the maximum channel spread L . For convenience, we set $T_t = K_2(N + N_c)$, and choose the training preamble sent by the BD as $x_t[n] = 1$, for $n = 0, \dots, T_t - 1$. The receiver can estimate D by autocorrelating the received signal $y[n]$, which is similar to the estimation of D_h as in (28) and thus omitted herein.

Utilizing the repeating structure of $y_d[n]$ in (10) and $y_b[n]$ in (12), we construct the metric

$$Q[l] = \frac{1}{K_2(N_c - l)} \sum_{k=0}^{K_2-1} \sum_{n=0}^{N_c-1-l} \left| y[n+l+k(N+N_c)] - y[n+l+N+k(N+N_c)] \right|^2. \quad (29)$$

For typical case of $N_c \gg L$, $Q[l]$ is distributed as $Q[l] \sim \mathcal{CN}(\tilde{\mu}_u(l), \tilde{\sigma}_u^2(l))$, with the mean value

$$\tilde{\mu}_u^2(l) = \begin{cases} \frac{2\sigma^2}{N_c-l} [(L_f - l)(\gamma_d + \gamma) + (L_b - L_f)\gamma + N_c - L_b], & \text{if } l < L_f < L_b \\ \frac{2\sigma^2}{N_c-l} [(L_b - l)(\gamma_d + \gamma) + (L_f - L_b)\gamma_d + N_c - L_f], & \text{if } l < L_b < L_f \\ \frac{2\sigma^2}{N_c-l} [(L_b - l)\gamma + N_c - L_b], & \text{if } L_f < l < L_b \\ \frac{2\sigma^2}{N_c-l} [(L_f - l)\gamma_d + N_c - L_f], & \text{if } L_b < l < L_f \\ 2\sigma^2, & \text{if } l \geq L. \end{cases} \quad (30)$$

and the variance value

$$\tilde{\sigma}_u^2(l) = \begin{cases} \frac{4\sigma^4}{K_2(N_c-l)^2} [(L_f - l)(\gamma_d + \gamma + 1)^2 + (L_b - L_f)(\gamma + 1)^2 + N_c - L_b], & \text{if } l < L_f < L_b \\ \frac{4\sigma^4}{K_2(N_c-l)^2} [(L_b - l)(\gamma_d + \gamma + 1)^2 + (L_f - L_b)(\gamma_d + 1)^2 + N_c - L_f], & \text{if } l < L_b < L_f \\ \frac{4\sigma^4}{K_2(N_c-l)^2} [(L_b - l)(\gamma + 1)^2 + N_c - L_b], & \text{if } L_f < l < L_b \\ \frac{4\sigma^4}{K_2(N_c-l)^2} [(L_f - l)(\gamma_d + 1)^2 + N_c - L_f], & \text{if } L_b < l < L_f \\ \frac{4\sigma^4}{K_2(N_c-l)^2}, & \text{if } l \geq L. \end{cases} \quad (31)$$

Clearly, when $l \geq L$, the metric $Q[l]$ is almost zero due to pure noise remaining in the difference signal; otherwise, $Q[l]$ is relatively large due to signal components. Therefore, the maximum channel spread L can be estimated by using Algorithm 1, shown in the above table.

Third, we consider the estimation of the average signal power σ_u^2 when the BD is backscattering. Using the estimated \hat{L} , the parameter σ_u^2 is estimated as

$$\hat{\sigma}_u^2 = \frac{1}{N_c} \sum_{n=0}^{N_c-1} \left| y[n + \hat{L}] - y[n + \hat{L} + N] \right|^2. \quad (32)$$

Algorithm 1 : Algorithm for estimating L

```

1: Initialization: some positive constant  $\epsilon$ .
2: for  $l = 0, \dots, N_c - 1$  do
3:   Compute  $Q[l]$  in (29).
4:   if  $Q[l] \leq 2\epsilon\sigma^2$ , then
5:     Obtain  $\hat{L} = l$ .
6:   end if
7: end for
8: return  $\hat{L}$ .

```

V. TRANSCIVER DESIGN FOR MULTI-ANTENNA RECEIVER

In this section, we study the transceiver design for an AmBC system with a receiver equipped with M antennas, for $M > 1$. We use the same BD waveform (i.e., transmitter) design as that for the single-antenna system studied in Section III, to maintain the ability of direct-link interference cancellation and information decoding by leveraging the repeating structure of the relevant signals due to CP. We thus focus on the optimal receiver design for the case of multi-antenna receiver in this section. The objective of the multi-antenna receiver is to detect the BD information bits, by processing the signals received at M antennas jointly and then making the final decision based on the calculated statistic. In the following, the test statistic is first constructed, and then the optimal detector is obtained.

A. Construction of Test Statistic

Similar to Section III-B, we construct the following intermediate signal based on the signal received by the m -th antenna, $m = 1, \dots, M$, at the receiver,

$$z_m[n] \triangleq y_m[n] - y_m(n+N) = \begin{cases} v_m[n], & \text{if } B = 0, \\ u_m[n] + v_m[n], & \text{if } B = 1, \end{cases} \quad (33)$$

where the signal $u_m[n] = 2\alpha g_m \sqrt{p} \sum_{l=0}^{L_h-1} s(n-l)h(l)$ and the noise $v_m[n] = w_m[n] - w_m(n+N)$. The signal $u_m[n]$ follows CSCG distribution with zero mean and variance given by

$$\sigma_{u,m}^2 = 4p|\alpha|^2 |g_m|^2 \sum_{l=0}^{L_h-1} |h[l]|^2. \quad (34)$$

And the noise follows that $v_m[n] \sim \mathcal{CN}(0, \sigma_v^2)$. We define the detection SNR of the m -th antenna as

$$\gamma_m \triangleq \frac{\sigma_{u,m}^2}{\sigma_v^2} = \frac{2p|\alpha|^2 |g_m|^2 \sum_{l=0}^{L_h-1} |h[l]|^2}{\sigma_v^2}. \quad (35)$$

We then construct the following test statistic for each receiver antenna m ,

$$R_m = \frac{1}{J\sigma_v^2} \sum_{n=L-1}^{N_c+D-1} |z_m[n]|^2. \quad (36)$$

We further construct the following test statistic for the final decision,

$$\tilde{R} = \sum_{m=1}^M \theta_m R_m, \quad (37)$$

where the combination weights θ_m 's are subject to $\sum_{m=1}^M \theta_m^2 = 1$ and $\theta_m \geq 0, \forall m$. Denote $\boldsymbol{\theta} = [\theta_1 \ \theta_2 \ \dots \ \theta_M]^T$.

We assume that the channels for different antennas at the receiver are mutually independent. Similar to Lemma 1, when the repeating length J is large, the conditional distribution of the test statistic \tilde{R} is given by

$$\tilde{R} = \begin{cases} \tilde{R}|_{B=0} \sim \mathcal{N}(\tilde{\mu}_0, \tilde{\sigma}_0^2), & \text{if } B = 0, \\ \tilde{R}|_{B=1} \sim \mathcal{N}(\tilde{\mu}_1, \tilde{\sigma}_1^2), & \text{if } B = 1, \end{cases} \quad (38)$$

where the values of mean are

$$\tilde{\mu}_0 = \tilde{\mu}_0(\boldsymbol{\theta}) = \sum_{m=1}^M \theta_m, \quad \tilde{\mu}_1 = \tilde{\mu}_1(\boldsymbol{\theta}) = \sum_{m=1}^M \theta_m(\gamma_m + 1), \quad (39)$$

and the values of variance are

$$\tilde{\sigma}_0^2 = \tilde{\sigma}_0^2(\boldsymbol{\theta}) = \frac{1}{J}, \quad \tilde{\sigma}_1^2 = \tilde{\sigma}_1^2(\boldsymbol{\theta}) = \frac{1}{J} \sum_{m=1}^M \theta_m^2 (\gamma_m + 1)^2. \quad (40)$$

B. Optimal Detector Design

For the optimal receiver design, the objective is to find the optimal combination weights $\boldsymbol{\theta}$ and detection threshold $\tilde{\epsilon}$, such that the following BER is minimized.

$$\tilde{P}_e(\boldsymbol{\theta}, \tilde{\epsilon}) = \frac{1}{2}P_{fa}(\boldsymbol{\theta}, \tilde{\epsilon}) + \frac{1}{2}P_{md}(\boldsymbol{\theta}, \tilde{\epsilon}) = \frac{1}{2}\mathcal{Q}\left(\sqrt{J}(\tilde{\epsilon} - \tilde{\mu}_0(\boldsymbol{\theta}))\right) + \frac{1}{2}\mathcal{Q}\left(\frac{\tilde{\mu}_1(\boldsymbol{\theta}) - \tilde{\epsilon}}{\sqrt{\tilde{\sigma}_1^2(\boldsymbol{\theta})}}\right). \quad (41)$$

That is, the optimization problem can be formulated as follows

$$(P2) \quad \min_{\boldsymbol{\theta}, \tilde{\epsilon}} \tilde{P}_e(\boldsymbol{\theta}, \tilde{\epsilon}) = \frac{1}{2}\mathcal{Q}\left(\sqrt{J}(\tilde{\epsilon} - \tilde{\mu}_0(\boldsymbol{\theta}))\right) + \frac{1}{2}\mathcal{Q}\left(\frac{\tilde{\mu}_1(\boldsymbol{\theta}) - \tilde{\epsilon}}{\sqrt{\tilde{\sigma}_1^2(\boldsymbol{\theta})}}\right) \quad (42a)$$

$$\text{s. t.} \quad \sum_{m=1}^M \theta_m^2 = 1, \quad (42b)$$

$$\theta_m \geq 0, \quad m = 1, \dots, M \quad (42c)$$

$$\tilde{\epsilon} > 0. \quad (42d)$$

It is difficult to solve (P2) directly, due to the complicated interplay between $\boldsymbol{\theta}$ and $\tilde{\epsilon}$ in the \mathcal{Q} -function. Before simplifying (P2), we have the following proposition.

Proposition 1. Given $\boldsymbol{\theta}$, the optimal threshold for minimizing BER is given by

$$\tilde{\epsilon}^*(\boldsymbol{\theta}) = \frac{\tilde{\mu}_0(\boldsymbol{\theta})\tilde{\sigma}_1^2(\boldsymbol{\theta}) - \tilde{\mu}_1(\boldsymbol{\theta}) + \sqrt{\tilde{\sigma}_1^2(\boldsymbol{\theta})(\tilde{\mu}_1(\boldsymbol{\theta}) - \tilde{\mu}_0(\boldsymbol{\theta}))^2 + \tilde{\sigma}_1^2(\boldsymbol{\theta})(\tilde{\sigma}_1^2(\boldsymbol{\theta}) - 1) \log(\tilde{\sigma}_1^2(\boldsymbol{\theta}))}}{\tilde{\sigma}_1^2(\boldsymbol{\theta}) - 1}. \quad (43)$$

And the corresponding minimum BER is given by

$$\tilde{P}_{e,\min}(\boldsymbol{\theta}) = \frac{1}{2}\mathcal{Q}(f_1(\boldsymbol{\theta})) + \frac{1}{2}\mathcal{Q}(f_2(\boldsymbol{\theta})), \quad (44)$$

where the two positive-valued functions of $\boldsymbol{\theta}$ in the above are given by

$$f_1(\boldsymbol{\theta}) = \sqrt{J}(\tilde{\epsilon}^*(\boldsymbol{\theta}) - \tilde{\mu}_0(\boldsymbol{\theta})), \quad (45)$$

$$f_2(\boldsymbol{\theta}) = \frac{\tilde{\mu}_1(\boldsymbol{\theta}) - \tilde{\epsilon}^*(\boldsymbol{\theta})}{\sqrt{\tilde{\sigma}_1^2(\boldsymbol{\theta})}}, \quad (46)$$

with $\tilde{\mu}_0(\boldsymbol{\theta})$, $\tilde{\mu}_1(\boldsymbol{\theta})$ and $\tilde{\sigma}_1^2(\boldsymbol{\theta})$ given in (39) and (40), respectively.

Proof: It is noted that given $\boldsymbol{\theta}$, the BER is minimized when the threshold $\tilde{\epsilon}(\boldsymbol{\theta})$ is chosen as the intersection point of the two conditional PDFs $p(\tilde{R}|_{B=0}, \boldsymbol{\theta})$ and $p(\tilde{R}|_{B=1}, \boldsymbol{\theta})$. Following the same steps as the proof of Theorem 1, this proposition is proved. \blacksquare

From the condition $p(\tilde{R}|_{B=0}, \boldsymbol{\theta}) = p(\tilde{R}|_{B=1}, \boldsymbol{\theta})$, we further have

$$f_1^2(\boldsymbol{\theta}) = f_2^2(\boldsymbol{\theta}) + \ln(\tilde{\sigma}_1^2(\boldsymbol{\theta})). \quad (47)$$

From Proposition 1, the optimal combination weights $\boldsymbol{\theta}$ are chosen to minimize the conditional BER $\tilde{P}_{e,\min}(\boldsymbol{\theta})$ in (44). From (47), Problem (P2) is equivalent to the following optimization problem,

$$\text{(P2-Equi.)} \quad \min_{\boldsymbol{\theta}} \tilde{P}_{e,\min}(\boldsymbol{\theta}) = \frac{1}{2}\mathcal{Q}\left(\sqrt{f_2^2(\boldsymbol{\theta}) + \ln(\tilde{\sigma}_1^2(\boldsymbol{\theta}))}\right) + \frac{1}{2}\mathcal{Q}(f_2(\boldsymbol{\theta})) \quad (48a)$$

$$\text{s. t.} \quad \sum_{m=1}^M \theta_m^2 = 1, \quad (48b)$$

$$\theta_m \geq 0, \quad m = 1, \dots, M. \quad (48c)$$

The objective function of (P2-Equi.) is complicated, and the optimal $\boldsymbol{\theta}^*$ can be obtained by $(M-1)$ -dimensional search. Since the number of receive antennas M is small or moderate in practice, due

to limited size of receiver, the complexity of $(M - 1)$ -dimensional search is acceptable.

In Section VII, we will numerically compare the BER performance of the optimal combining weights θ^* , to those of three traditional combining schemes including the maximum-ratio-combining (MRC), equal-gain-combining (EGC), and selection-combining (SC). The traditional schemes determine the combination weights based on only the SNRs of individual receive branches, thus are simpler to obtain. Numerical results will show that compared to the scheme using the optimal combination weights θ^* , the MRC, EGC and SC schemes suffer from negligible SNR losses in terms of BER performance, thus are good suboptimal and low-complexity combining schemes in practice.

VI. PERFORMANCE ANALYSIS

In this section, we analyze the rate performance and the BER performance for the proposed transceiver design.

A. Rate Performance

Recall the designed BD waveform in (8) and (9). Since the time duration of each BD symbol is equal to $K(N + N_c)$ sampling periods, the BD rate is obtained as

$$R_{\text{BD}} = \frac{f_s}{K(N + N_c)}. \quad (49)$$

We observe that there is a trade-off between the data rate and the reliability, for different choices of BD symbol periods. For larger K , the BD data rate is lower, but the detection reliability at the receiver improves, since more signal samples are available for detection decision; and vice versa.

B. BER Performance for Single-recv-antenna System

We analyze the effect of the CP length N_c and the channel spread L on the BER performance for the single-antenna receiver case as follows.

From Theorem 1, the minimum BER $P_{e,\min}$ is rewritten as

$$P_{e,\min}(J, \gamma) = \frac{1}{2} \mathcal{Q}(f_1(J, \gamma)) + \frac{1}{2} \mathcal{Q}(f_2(J, \gamma)), \quad (50)$$

with the two quantities

$$f_1(J, \gamma) = \frac{\sqrt{J}}{\gamma(\gamma + 2)} \left((\gamma + 1) \sqrt{\gamma^2 + \frac{2\gamma(\gamma + 2) \ln(\gamma + 1)}{J}} - \gamma \right), \quad (51)$$

$$f_2(J, \gamma) = \frac{\sqrt{J}}{\gamma(\gamma + 2)} \left(\gamma^2 + \gamma - \sqrt{\gamma^2 + \frac{2\gamma(\gamma + 2) \ln(\gamma + 1)}{J}} \right). \quad (52)$$

It can be further checked that $f_1(J, \gamma) > 0$ and $f_2(J, \gamma) > 0$.

From the condition $p(R|_{B=0}) = p(R|_{B=1})$, we have

$$f_1^2(J, \gamma) = f_2^2(J, \gamma) + 2 \ln(\gamma + 1) > f_2^2(J, \gamma). \quad (53)$$

The minimum BER $P_{e,\min}$ is thus rewritten as

$$P_{e,\min}(J, \gamma) = \frac{1}{2} \mathcal{Q} \left(\sqrt{f_2^2(J, \gamma) + 2 \ln(\gamma + 1)} \right) + \frac{1}{2} \mathcal{Q} (f_2(J, \gamma)). \quad (54)$$

Moreover, we have the following proposition on the effect of N_c and L on the BER performance.

Proposition 2. Given γ , the minimum BER $P_{e,\min}$ decreases, as either N_c increases or L decreases.

Proof: It can be checked that given γ , $f_2(J, \gamma)$ is an increasing function of J . The minimum BER $P_{e,\min}$ decrease as J increases, due to the fact that \mathcal{Q} -function is a decreasing function of its argument. Since $J = N_c + D - L + 1$, this proposition is proved. \blacksquare

Next, we analyze the effect of the detection SNR γ on the BER performance. We focus on the typical case that the (decimal) SNR γ is sufficiently large such that $\frac{1}{\gamma} \approx 0$.

From (50), the minimum probability of false alarm $P_{fa,\min}$ is approximated as

$$P_{fa,\min}(J, \gamma) \approx \mathcal{Q} \left(\sqrt{J + 2 \ln(\gamma + 1)} \right), \quad (55)$$

and the minimum probability of missing detection $P_{md,\min}$ is approximated as

$$P_{md,\min}(J, \gamma) \approx \mathcal{Q} \left(\sqrt{J} \right), \quad (56)$$

where the approximation in (56) is from the inequality $\log(1+x) \leq x$, $\forall x > -1$, and the assumption that $\frac{1}{\gamma} \approx 0$.

Given J , the minimum probability of false alarm $P_{fa,\min}$ dominates the minimum BER $P_{e,\min} = \frac{1}{2} P_{fa,\min} + \frac{1}{2} P_{md,\min}$, since the minimum probability of missing detection $P_{md,\min}$ approximately equals the constant $\mathcal{Q} \left(\sqrt{J} \right)$. Note $P_{fa,\min}$ decreases as γ increases, due to the fact that the \mathcal{Q} -function is a monotonically decreasing function. Thus we directly have the following proposition.

Proposition 3. Given N_c and L , for a decimal SNR γ that is sufficiently large such that $\frac{1}{\gamma} \approx 0$, the BER $P_{e,\min}$ decreases as the SNR γ increases.

Clearly, Proposition 3 coincides with the intuition that the BER decreases as the SNR γ increases.

C. BER Performance for Multiple-receive-antenna System

With the optimal combination weights $\boldsymbol{\theta}^*$, the minimum BER is obtained from (48a) as

$$\tilde{P}_{e,\min}(\boldsymbol{\theta}^*) = \frac{1}{2} \mathcal{Q} \left(\sqrt{f_2^2(\boldsymbol{\theta}^*) + \ln(\tilde{\sigma}_1^2(\boldsymbol{\theta}^*))} \right) + \frac{1}{2} \mathcal{Q}(f_2(\boldsymbol{\theta}^*)). \quad (57)$$

VII. NUMERICAL RESULTS

In this section, we provide simulation results to evaluate the performance of the proposed transceiver design. Suppose that the OFDM signal bandwidth or sampling frequency f_s is 10MHz. The channel taps are modeled as statistically independent Gaussian random variables with zero mean (Rayleigh fading) and an exponentially decaying power delay profile. We set $\tau_g = 1$, and assume that the channel gain $\mathbb{E}[|g_m|^2] = \frac{c^2}{4\pi D_{rd}^2 f_c^2}, \forall m = 1, \dots, M$, where the light speed $c = 3 \times 10^8$ meters per second, the carrier frequency $f_c = 900$ MHz, and the distance between the BD and the receiver $D_{rd} = 0.5$ meter (m) which implies the channel propagation delay $D_g = \lfloor \frac{D_{rd} f_s}{c} \rfloor = 0$. We set the channel parameters $D_f = 16, D_h = 16$, and $\tau_f = 4, \tau_h = 6$, which implies $D = 16$ and $L = 22$. We set the reflection coefficient $\alpha = 0.3 + 0.4j$, which implies that about 25% incident power is reflected by the BD. We assume that the BD adopts binary phase shift keying (BPSK) modulation. We set the number of subcarriers $N = 512$ and the CP length $N_c = 64$. The following numerical results are based on 10^8 Monte Carlo simulations each with randomly generated channels.

A. Timing Estimation for AmBC System

In this subsection, we evaluate the performance of timing estimation for AmBC systems. We set the parameter $\epsilon = 1.5$ for Algorithm 1.

Fig. 6 plots the normalized mean-square-error (MSE) versus the SNR γ , for different synchronization time K_1 's or K_2 's. For estimating D_h by the BD using the conventional autocorrelation based method, the MSE is about 0.01, since the SNR at the BD is about 20 dB larger than the SNR γ at the receiver due to the small reflection coefficient α and the channel attenuation from the BD to the receiver. For autocorrelation based estimation of D at the receiver, the MSE decreases quickly as the SNR γ increases. We observe that the MSE curve has a floor for the SNR $\gamma > 15$ dB, which verifies that the performance of autocorrelation based synchronization for OFDM signals is dominated by the delay profile and not sensitive to the noise level [33]. For estimating L at the receiver, the MSE also decreases as the SNR γ increases. In particular, we observe that for the SNR $\gamma = 30$ dB, the normalized MSE is 0.016, 0.01, and 0.008 for $K_2 = 1, 2$, and 3, respectively.

For estimating D_h, D and L , we observe that the normalized MSE becomes smaller for longer synchronization time (i.e., larger K_1 or K_2), which implies that it is sufficient to use one or two OFDM symbols for timing synchronization in practice. Since we have $N_c \gg D_h$ and $N_c \gg L$ in

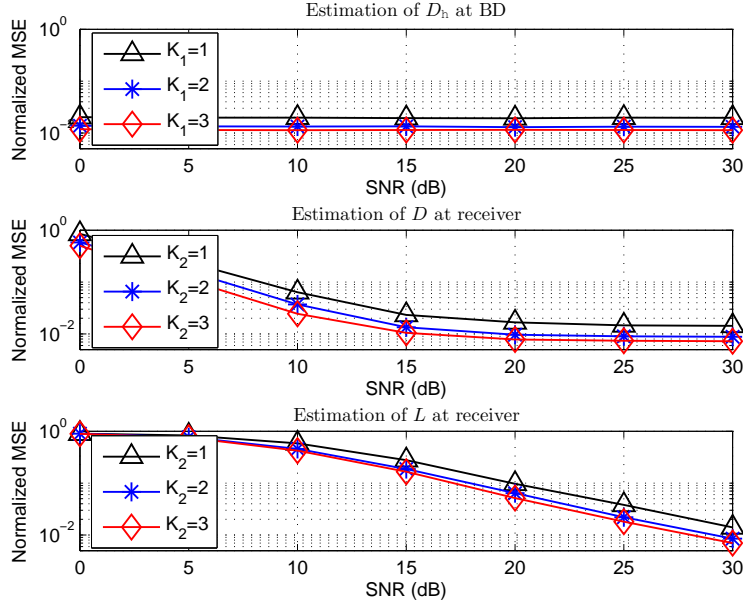


Fig. 6: Normalized MSE comparison for estimating D_h , D and L .

practice, the MSE performance achieved by the proposed method is sufficient for implementation. Thus we assume perfect timing synchronization at the BD and the receiver in the subsequent simulations.

B. Performance Comparison for Case of Single-antenna Receiver

In this subsection, we evaluate the BER performance for the case of a single-antenna receiver. For performance comparison, we consider the energy detector in [4] as a benchmark, in which, for the case of $K = 1$, the BD reflects for bit ‘1’ and keeps silent for bit ‘0’, and the receiver detects the BD bit by distinguishing between two different energy levels of the received signal $y[n]$, given by

$$\hat{R} \triangleq \frac{1}{N + N_c} \sum_{n=0}^{N+N_c-1} |y[n]|^2. \quad (58)$$

Differential coding is used in [4] to exempt the receiver from knowing the extra mapping from the power levels to the bits.

1) *Scenario of Fixed Distance between BD and Receiver:* We fix the distance between the BD and the receiver as $D_{rd} = 0.5$ m.

Fig. 7 plots the BER versus the average SNR, by using the proposed optimal detector and the conventional energy detector, for different BD symbol duration K 's. We observe that by using the proposed optimal detector, the BER for $K = 1$ decreases dramatically from 0.12 to 1.6×10^{-4} ,

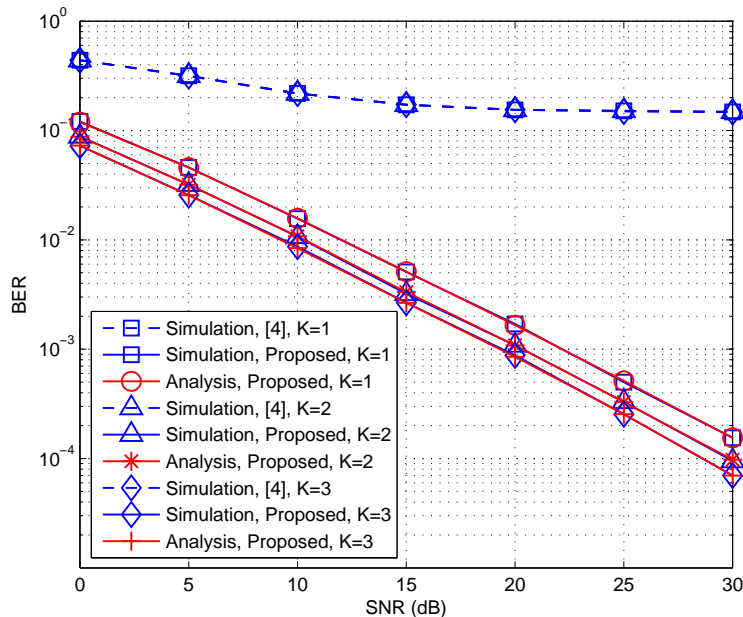


Fig. 7: BER comparison for both proposed and conventional designs.

as the average SNR increases from 0 dB to 30 dB. Moreover, simulation results verify the trade-off between the BD rate and the reliability of signal recovery. With the parameter setting in our simulations, the BD rate is 19.5 Kbps, 9.8 Kbps and 6.5 Kbps, for $K = 1, 2$ and 3 , respectively. We observe that the BER decreases for larger K . Specifically, for a BER level of 0.001, the system achieves an SNR gain of 2 dB and 3 dB for $K = 2$ and 3 , respectively, compared to the case of $K = 1$. Also, we observe that the simulated BERs coincide with the analytical BERs, which verifies Theorem 1.

In contrast, by using the conventional energy detector, the BER decreases slowly, saturating at a high BER around 0.16. This is explained as follows. The energy detector decodes the BD bit by treating the strong direct-link interference from the RF source as noise. Since the direct-link interference is typically much stronger than the backscattered signal, this results in very low decoding SNR and thus high BER floor.

2) *Scenario of Varying Distance between BD and Receiver:* In this example, we vary the distance D_{rd} between the BD and the receiver. We set $K = 1$.

Fig. 8 plots the BER versus the distance D_{rd} , for both the proposed transceiver and the conventional energy detector [4]. In general, the BER increases as D_{rd} increases. For the proposed transceiver design, the BER is around 0.001, 0.01 and 0.1, for the distance $D_{rd} = 1.4, 4$ and 14 meters. While for the benchmark scheme, the BER is around 0.15, 0.4 and 0.5, for the distance $D_{rd} = 0.5, 2$ and 6 meters. It is concluded that the proposed design enhances the BER performance as well as the

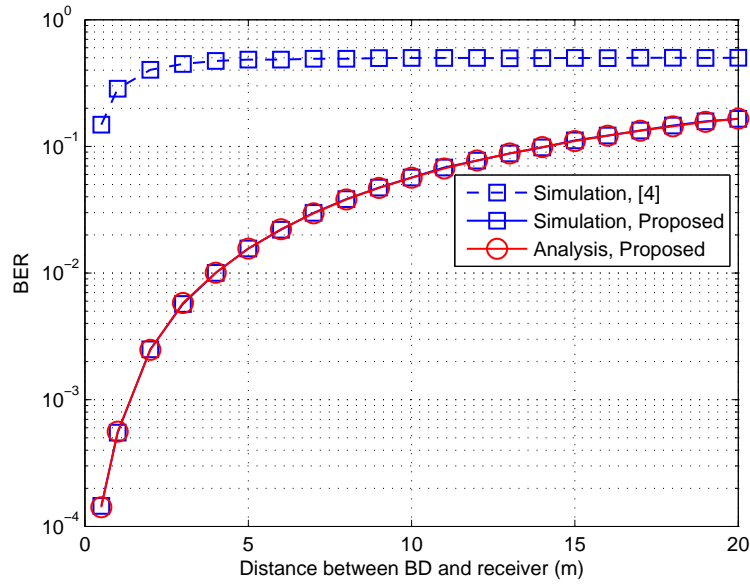


Fig. 8: BER comparison for different distances between BD and receiver.

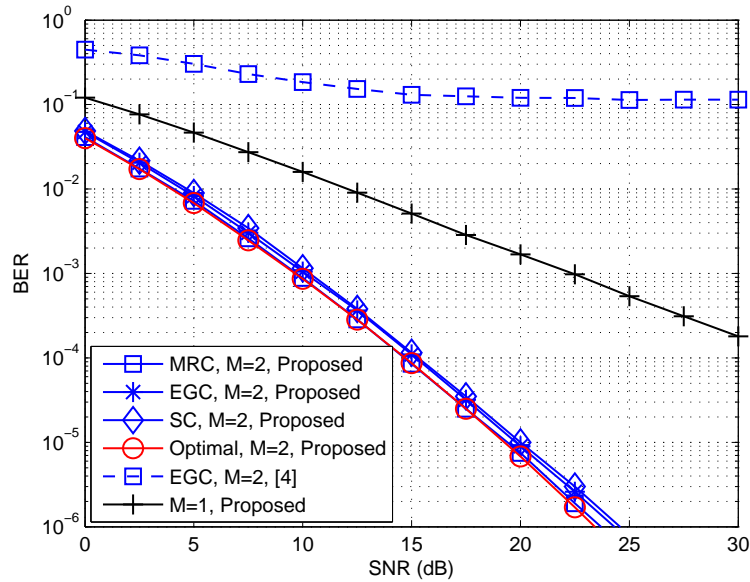


Fig. 9: BER comparison for different combining schemes, for $M = 2$.

operating range significantly, compared to the conventional energy detector.

C. Performance Comparison for Case of Multi-antenna Receiver

In this subsection, we evaluate the BER performance for the case of a multi-antenna receiver. Fig. 9 compares the BER of different combining schemes, for the number of receiver antennas $M = 2$. The optimal combining weights are obtained by one-dimensional search, and the search-step is set to be 0.001. First, we observe that by using two antennas at the receiver, the proposed

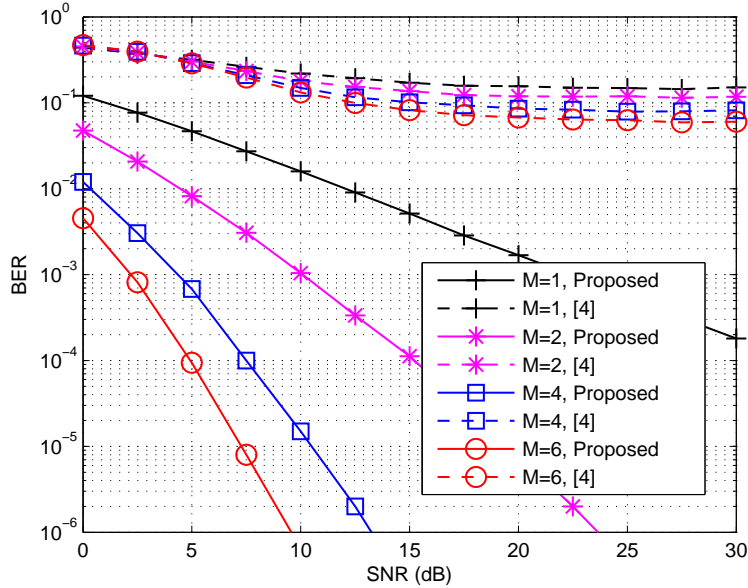


Fig. 10: BER comparison for different M 's, with EGC.

transceiver achieves an SNR gain of about 12 dB at a BER level of 0.001, compared to the case of a single-antenna receiver. This verifies that the receive diversity can decrease the BER significantly. Second, the BER performance difference for different combining schemes is small. In particular, at a BER level of 0.001, compared to the optimal combining scheme, the MRC, EGC and SC schemes suffer from an SNR loss of 0.2 dB, 0.5 dB, and 0.6 dB, respectively. For the conventional energy detector, the BER decreases very slowly with SNR, saturating at a high BER around 0.11.

The MRC and SC schemes require the SNR information of signals received at each antenna, which requires additional estimation. The above observations imply that the simple EGC scheme is suitable for the scenarios with unknown SNRs, since the EGC scheme does not require the SNR information. The EGC scheme can also reduce the computational complexity, as it avoids the search for optimal combination weights.

Fig. 10 compares the BER with different number of receiver antennas M 's, for the EGC scheme. First, we observe that the BER decreases quickly as M increases. In particular, at a BER level of 0.001, the system achieves an SNR gain of 12 dB, 18 dB, and 20 dB, for $M = 2, 4, 6$, respectively, compared to the single-antenna case. This implies that the incremental SNR gain becomes smaller as M increases. We also observe that the BER improvement becomes less significant as M increases. This is in accordance with the BER performance of receiver diversity via EGC [26]. For the conventional energy detector [4], the BER decreases slowly as M increases, due to the strong direct-link interference.

VIII. CONCLUSIONS

This paper has studied a new backscatter communication system over ambient OFDM carriers in the air. We first establish the system model for such system from a spread-spectrum modulation perspective, upon which a novel joint design for BD waveform and receiver detector is proposed. For the system with a single-antenna receiver, we construct a test statistic that cancels out the direct-link interference by exploiting the repeating structure of the relevant signals due to the use of CP, and propose the optimal maximum-likelihood detector to recover the BD information bits, for which the optimal detection threshold is obtained in closed-form expression. For the system with a multi-antenna receiver, we further construct a new test statistic and derive the corresponding optimal detector. To perform optimal detection, the receiver requires to estimate only the strength of the backscatter channel, instead of the complete information of the relevant channels, leading to reduced receiver complexity. We also propose efficient algorithms for timing synchronization in the considered AmBC system. The effect of various system parameters on the transmission rate and detection performance is analyzed. Simulation results have shown that the proposed design outperforms the conventional design based on energy detection, in terms of transmission rate, BER performance and operating range. Also, the results have shown that the proposed timing synchronization method is practically valid and efficient, and the deployment of multiple receive antennas at the receiver can enhance the BER performance significantly. The proposed transceiver design has great potential for applications in the next-generation low-power IoT systems.

APPENDIX A

PROOF TO LEMMA 1

Under the condition of $B = 1$, from CLT [32], we have that $R|_{B=1} \sim \mathcal{N}(\mu_1, \sigma_1^2)$. The mean value is first given by

$$\begin{aligned}
 \mu_1 &\triangleq \frac{1}{J\sigma_v^2} \sum_{n=L-1}^{N_c-1} \mathbb{E}[|u[n] + v[n]|^2] \\
 &\stackrel{(a)}{=} \frac{\mathbb{E}[|u[n] + v[n]|^2]}{\sigma_v^2} \\
 &\stackrel{(b)}{=} \frac{\mathbb{E}[|u[n]|^2] + \mathbb{E}[|v[n]|^2]}{\sigma_v^2} \\
 &\stackrel{(c)}{=} \gamma + 1,
 \end{aligned} \tag{59}$$

where (a) is from the fact that random variables $u[n]$'s are i.i.d. and $v[n]$'s are also i.i.d., (b) is from the mutual independence between $u[n]$ and $v[n]$ for any n , and (c) is from the facts that $\mathbb{E}[|u[n]|^2] = \gamma\sigma_v^2$ and $\mathbb{E}[|v[n]|^2] = \sigma_v^2$.

Next, the variance value is given by

$$\begin{aligned}
\sigma_1^2 &\triangleq \frac{1}{J^2\sigma_v^4} \mathbb{E} \left[\left| \sum_{n=L-1}^{N_c-1} (|u[n] + v[n]|^2 - \mathbb{E}[|u[n] + v[n]|^2]) \right|^2 \right] \\
&\stackrel{(a)}{=} \frac{1}{J^2\sigma_v^4} \mathbb{E} \left[\sum_{n=L-1}^{N_c-1} (|u[n] + v[n]|^2 - (\sigma_u^2 + \sigma_v^2))^2 \right] \\
&\stackrel{(b)}{=} \frac{\mathbb{E} \left[(|u[n] + v[n]|^2 - (\sigma_u^2 + \sigma_v^2))^2 \right]}{J\sigma_v^4} \\
&\stackrel{(c)}{=} \frac{\mathbb{E}[|u[n]|^4] + \mathbb{E}[|v[n]|^4] - (\sigma_u^2 - \sigma_v^2)^2}{J\sigma_v^4} \\
&\stackrel{(d)}{=} \frac{(\gamma + 1)^2}{J},
\end{aligned} \tag{60}$$

where (a) is from (59), (b) is from the fact that random variables $u[n]$'s are i.i.d. and $v[n]$'s are also i.i.d., (c) is from the mutual independence between $u[n]$ and $v[n]$ for any n , and (d) is from the facts that $\mathbb{E}[|u[n]|^4] = 2\sigma_u^4$, and $\mathbb{E}[|v[n]|^4] = 2\sigma_v^4$.

Also, the distribution under the condition of $B = 0$ can be proved in a similar way.

APPENDIX B

PROOF TO THEOREM 1

As can be seen from the shadow area in Fig. 5, the BER is minimized when the threshold ϵ is chosen as the intersection point of the two conditional PDFs $p(R|_{B=0})$ and $p(R|_{B=1})$. From (19), the optimal ϵ^* is thus the solution to the following equation,

$$\frac{1}{\sqrt{2\pi\sigma_0^2}} \exp\left(-\frac{(t-\mu_0)^2}{2\sigma_0^2}\right) = \frac{1}{\sqrt{2\pi\sigma_1^2}} \exp\left(-\frac{(t-\mu_1)^2}{2\sigma_1^2}\right). \tag{61}$$

Define the constant $C \triangleq (\gamma + 1)^2$. After taking the logarithm on both sides of (61) and some manipulations, the equation (61) is simplified as

$$\frac{C-1}{2}T^2 + (\mu_1 - C\mu_0)T + \frac{C\mu_0^2 - \mu_1^2 - \sigma_1^2 \ln C}{2} = 0. \tag{62}$$

Solving the above equation yields the optimal threshold

$$\epsilon^* = \frac{C\mu_0 - \mu_1 + \sqrt{C(\mu_1 - \mu_0)^2 + (C-1)\sigma_1^2 \ln C}}{C-1}. \tag{63}$$

Substituting (20) and (21) in (63), the optimal detection threshold is obtained as in (26), and the corresponding minimum BER is given in (27).

REFERENCES

- [1] G. Yang and Y.-C. Liang, "Backscatter communications over ambient OFDM signals: transceiver design and performance analysis," in *Proc. of IEEE Globecom*, Washington DC, USA, Dec. 2016, pp. 1–6.
- [2] S. Bi, C. K. Ho, and R. Zhang, "Wireless powered communication: opportunities and challenges," *IEEE Commun. Mag.*, vol. 53, no. 4, pp. 117–125, Apr. 2015.
- [3] S. Bi, Y. Zeng, and R. Zhang, "Wireless powered communication networks: an overview," *IEEE Wireless Commun.*, vol. 23, no. 4, pp. 10–18, Apr. 2016.
- [4] V. Liu, A. Parks, V. Talla, S. Gollakota, D. Wetherall, and J. R. Smith, "Ambient backscatter: wireless communication out of thin air," in *Proc. of ACM SIGCOMM*, Hong Kong, China, Jun. 2013, pp. 1–13.
- [5] Y.-C. Liang, K.-C. Chen, G. Y. Li, and P. Mahonen, "Cognitive radio networking and communications: An overview," *IEEE Trans. Veh. Technol.*, vol. 60, no. 7, pp. 3386–3407, Sept. 2011.
- [6] D. M. Dobkin, *The RF in RFID: Passive UHF RFID in Practice*. Elsevier, 2007.
- [7] A. Sample, D. Yeager, P. Powledge, and J. Smith, "Design of a passively-powered, programmable sensing platform for UHF RFID systems," in *Proc. of IEEE Int. Conf. on RFID*, Grapevine, TX, Mar. 2007, pp. 149–156.
- [8] A. Parks and J. Smith, "Shifting through the airwaves: efficient and scalable multiband RF harvesting," in *Proc. of IEEE Conf. RFID*, Orlando, FL, USA, Apr. 2014, pp. 74–81.
- [9] H. Ishizaki, H. Ikeda, Y. Yoshida, T. Maeda, T. Kuroda, and M. Mizuno, "A battery-less WiFi-BER modulated data transmitter with ambient radio-wave energy harvesting," in *IEEE Symp. VLSI Circuits*, Kyoto, JP, Dec. 2011, pp. 162–163.
- [10] J. Qian, F. Gao, G. Wang, S. Jin, and H. Zhu, "Noncoherent detections for ambient backscatter system," *IEEE Trans. Wireless Commun.*, vol. 16, no. 3, pp. 1412–1422, Mar. 2017.
- [11] G. Wang, F. Gao, R. Fan, and C. Tellambura, "Ambient backscatter communication systems detection and performance analysis," *IEEE Trans. Commun.*, vol. 64, no. 11, pp. 4836–4846, Nov. 2016.
- [12] B. Kellogg, A. Parks, S. Gollakota, J. R. Smith, and D. Wetherall, "Wi-Fi backscatter: Internet connectivity for RF-powered devices," in *Proc. of ACM SIGCOMM*, Chicago, USA, Jun. 2014, pp. 1–12.
- [13] A. N. Parks, A. Liu, S. Gollakota, and J. R. Smith, "Turbocharging ambient backscatter communication," in *Proc. of ACM SIGCOMM*, Chicago, IL, USA, Aug. 2014, pp. 1–12.
- [14] D. Bharadia, K. Joshi, M. Kotaru, and S. Katti, "BackFi: High throughput WiFi backscatter," in *Proc. of ACM SIGCOMM*, London, UK, Aug. 2015, pp. 283–296.
- [15] P. Zhang, D. Bharadia, K. Joshi, and S. Katti, "Hitchhike: Practical backscatter using commodity WiFi," in *Proc. of ACM Conf. Embedded Netw. Sensor Sys.*, Stanford, CA, USA, Nov. 2016, pp. 259–271.
- [16] B. Kellogg, V. Talla, S. Gollakota, and J. R. Smith, "Passive Wi-Fi: Bringing low power to Wi-Fi transmissions," in *Proc. of USENIX Symposium on Networked Systems Design and Implementation (NSDI)*, Santa Clara, CA, USA, Mar. 2016, pp. 151–164.
- [17] V. Iyery, V. Tallay, B. Kellogg, S. Gollakota, and J. R. Smith, "Inter-technology backscatter: Towards internet connectivity for implanted devices," in *Proc. of ACM SIGCOMM*, Florianopolis, Brazil, Aug. 2016, pp. 356–369.
- [18] P. Zhang, M. Rostami, P. Hu, and D. Ganesan, "Enabling practical backscatter communication for on-body sensors," in *Proc. of ACM SIGCOMM*, Florianopolis, Brazil, Aug. 2016, pp. 370–383.
- [19] C. He and Z. J. Wang, "Closed-form BER analysis of non-coherent FSK in MISO double rayleigh fading/RFID channel," *IEEE Commun. Lett.*, vol. 15, no. 8, pp. 848–850, Aug. 2011.
- [20] C. Boyer and S. Roy, "Backscatter communication and RFID: coding, energy, and MIMO analysis," *IEEE Trans. Commun.*, vol. 62, no. 3, pp. 770–785, Mar. 2014.
- [21] N. B. Carvalho and etc., "Wireless power transmission: R&D activities within europe," *IEEE Trans. Microwave Theory Tech.*, vol. 62, no. 4, pp. 1031–1045, Apr. 2014.
- [22] A. J. S. Boaventura and N. B. Carvalho, "Extending reading range of commercial RFID readers," *IEEE Trans. Microwave Theory Tech.*, vol. 61, no. 1, pp. 633–640, Jan. 2013.
- [23] G. Yang, C. K. Ho, and Y. L. Guan, "Multi-antenna wireless energy transfer for backscatter communication systems," *IEEE J. Sel. Areas Commun.*, vol. 33, no. 12, pp. 2974–2987, Dec. 2015.

- [24] J. Kimionis, A. Bletsas, and J. N. Sahalos, "Increased range bistatic scatter radio," *IEEE Trans. Commun.*, vol. 62, no. 3, pp. 1091–1104, Mar. 2014.
- [25] K. Han and K. Huang, "Wirelessly powered backscatter communication network: Modeling, coverage and capacity," to appear in *IEEE Trans. Wireless Commun.* [Early Access].
- [26] A. Goldsmith, *Wireless Communications*. Cambridge Univ. Press, 2005.
- [27] C. Bryant and H. Sjöland, "A 2.45ghz ultra-low power quadrature front-end in 65nm CMOS," in *Proc. of IEEE Radio Frequency Integrated Circuits Symposium*, Montreal, QC, Canada, Jun. 2012, pp. 247–250.
- [28] C. Boyer and S. Roy, "Space time coding for backscatter RFID," *IEEE Trans. Wireless Commun.*, vol. 12, no. 5, pp. 2272–2280, May 2013.
- [29] R. Zhang and Y.-C. Liang, "Exploiting multi-antennas for opportunistic spectrum sharing in cognitive radio networks," *IEEE J. Select. Topics Signal Process.*, vol. 2, no. 1, pp. 88–102, Sept. 2008.
- [30] Y.-C. Liang, Y. Zeng, E. C. Y. Peh, and A. T. Hoang, "Sensing-throughput tradeoff for cognitive radio networks," *IEEE Trans. Wireless Commun.*, vol. 7, no. 4, pp. 1326–1336, Apr. 2008.
- [31] S. M. Kay, *Fundamentals of Statistical Signal Processing*. NJ, USA: Prentice Hall, 1993.
- [32] R. E. Walpole, R. H. Myers, S. L. Myers, and E. Ye, *Probability and Statistics for Engineers and Scientists*. Pearson, 9th edition.
- [33] J. G. Proakis and M. Salehi, *Digital Communications (5th Edition)*. NY, USA: McGraw-Hill, 2007.
- [34] IEEE Std 802.11a - 1999, Wireless LAN Medium Access Control (MAC) and Physical Layer (PHY) Specifications[S], 1999.
- [35] M. Morelli, C.-C. J. Kuo, and M.-O. Pun, "Synchronization techniques for orthogonal frequency division multiple access (OFDMA): A tutorial review," *Proceedings of the IEEE*, vol. 95, no. 7, pp. 1394–1427, Jul. 2007.